# Threshold Photoionization Study of $Fe(CO)_5$ versus ab Initio Calculations

**Celestino Angeli***

*Scuola Normale Superiore di Pisa, piazza dei Cavalieri 7, I-56100 Pisa, Italy*

**Gaston Berthier**

*Département de Physique, Ecole Normale Supérieure, Laboratoire d'Etude Théorique des Milieux Extrêmes, 24 rue Lhomond, 75231 Paris Cedex 05, France*

**Christian Rolando and Michel Sablier**

*Département de Chimie, Ecole Normale Supérieure, URA 1679 du CNRS, Processus d'Activation Moléculaire, 24 rue Lhomond, 75231 Paris Cedex 05, France*

**Christian Alcaraz**

*LURE, UMR CNRS−CEA−MEN, Centre Universitaire d'Orsay, 91405 Orsay Cedex, France*

**Odile Dutuit**

*Laboratoire de Physico-Chimie des Rayonnements (LPCR), URA 75 associée au CNRS, Centre Universitaire d'Orsay, Bât. 350, 91405 Orsay Cedex, France*

*Received: May 7, 1997; In Final Form: July 23, 1997*[⊗]

The threshold photoelectron spectrum (TPES) of iron pentacarbonyl $Fe(CO)_5$, is obtained over an energy range 5−35 eV using a synchrotron radiation source. Ab initio calculations at a level of theory more refined than Koopmans' theorem yield ionization potentials in better agreement with experiment and allow the assignment of the origin of most of the observed bands in the TPES on the basis of a decomposition in (quasi) local contributions. From the measured appearance threshold of $FeC^+$ the bond energy $D_0(Fe^+-C) = 84.2 \pm 4.1$ kcal/mol is obtained, and the enthalpy $\Delta H_f(Fe^+-C) = 366.0 \pm 6.0$ kcal/mol is derived.

## 1. Introduction

The growing interest in the field of gas-phase organometallic chemistry has given rise to a considerable amount of experimental and theoretical work devoted to the reactivity of metal ions.[1−3] This interest has opened a new approach to the field of ligated ionic metal species $ML^+$. A good understanding of how the electronic structure of $ML^+$ is related to its chemical reactivity is a help for studies dealing with the chemistry of ligand-bearing metal cations whose electronic structure is more complex and less known. Consequently, metal−ligand bond energies have been found to be a good parameter to assess whether a proposed reaction pathway is or is not energetically feasible. This explains why photodissociation is generally considered as a promising method for obtaining such informations.[4] Experimental and theoretical studies under well-controlled conditions are then necessary to examine properties and reactivities of ligated metal ions. In this context, the assignment of photoionization bands is particularly relevant as (i) first, it allows the correlation of electronic states of the $ML^+$ species to those of the metal or ligand part and then the deduction of the contributions involved in the metal or ligand moiety, and (ii) second, it allows the testing of new ab initio calculation methods. Iron carbonyl cations $Fe(CO)_x^+$ have been the subject of many experimental investigations mainly directed at determining the sequential bond dissociation energies through photoionization,[5−8] electron impact,[9,10] or collision-induced dissociation experiments.[11] Several studies have been performed on the photoelectron spectrum (PES) of $Fe(CO)_5$, both from experimental and theoretical points of view.[12−14] The only published threshold photoelectron spectrum (TPES) of iron pentacarbonyl is available in the narrow energy range 13−19 eV.[7] Comparatively few theoretical studies have been achieved concerning the bonding and the dissociation energies of $Fe(CO)^+$ and $Fe(CO)_2^+$ in their lowest electronic states.[15−17] In the experimental part of this work, we have compared the available photoelectron spectrum (PES) of iron pentacarbonyl, $Fe(CO)_5$, with the experimentally determined threshold photoelectron spectrum (TPES) in the energy range 5−35 eV, and in the theoretical part, we have investigated the correlation of computational results primarily based on Koopmans' theorem for ionization potentials (IPs) with experiment, in terms of band interpretations in the photoionization spectrum of $Fe(CO)_5$.

In addition, we present the appearance spectrum of $FeC^+$ as a function of deposited energy using a synchrotron radiation source. The $FeC^+$ cation may be a subject of astrophysical studies, as has been the case of a related species, FeCO.[18] Compounds containing metals are refractory compounds that are thought to exist in the interstellar clouds and/or circumstellar envelopes, but they are not yet detected. $FeC^+$ is likely involved in the iron chemistry of this medium, and experimental data are necessary for the characterization and laboratory modelization of its properties. The threshold appearance potential of $FeC^+$ is measured from the appearance spectrum; the corresponding bond energy is assigned and compared with a previous determination.[4]

In section 2 we shall present the experimental setup, in section 3 the previous theoretical estimates of the $Fe(CO)_5$ IPs, in section 4 the theory applied in this work, in section 5 the computational

[⊗] Abstract published in *Advance ACS Abstracts,* September 1, 1997.

S1089-5639(97)01534-X CCC: $14.00 

details, and in section 6 our interpretation of the $Fe(CO)_5$ TPE spectrum through Koopmans' theorem[19] (KT), its extension in terms of localized orbitals[20] (LOKT), and improvements taking into account repolarization and correlation effects. Finally, in section 7 the $FeC^+$ results will be discussed.

## 2. Experimental Section

Since the experimental apparatus has already been described in detail,[21] only a few points are needed here. Ions are produced by photoionization with synchrotron radiation at the Super-ACO Orsay storage ring. The VUV light is dispersed by a 3 m normal incidence Balzers monochromator equipped with a 1200 lines per mm Jobin-Yvon holographic grating. A LiF window is used up to its cutoff at 11.8 eV. Monochromatized light is refocused at the center of the ion source where the gaseous sample is introduced at an indicated pressure of $10^{-4}$ mbar. Electrons and ions are extracted in opposite directions by an electric field of about 4 V $cm^{-1}$. Threshold electrons are selected by a combination of angular and time-of-flight discrimination. A moderate energy resolution of about 30 meV is used here in order to get a higher detection efficiency. The remainder of the ion assembly includes a double octopole radio frequency ion guide, a quadrupole mass filter, and a multichannel plate detector.

The measurement of the signal corresponding to parent or fragment ions as a function of photon energy allows, in principle, the determination of both the ionization potential of the molecule and the appearance energy of the fragment ions.

## 3. Geometry of $Fe(CO)_5$

Calculations have indicated that the trigonal bipyramid is the most stable geometry for $d^8$ systems[22−24] even if the square pyramid geometry is not much higher in energy.[25] The equilibrium configuration of gaseous $Fe(CO)_5$ has been determined to be a trigonal bipyramid, corresponding to a $D_{3h}$ symmetry.[26,27] An energy difference of 0.6 kcal/mol was calculated for the intramolecular rearrangement of $Fe(CO)_5$ from the trigonal bipyramid geometry to the square pyramid geometry,[22] correlating well with the estimated value in the solid state.[28] Such calculations[22,23,25] strongly support Berry's mechanism[29] for the rearrangement process of $ML_5$ complexes. Under our experimental conditions, we can expect that the iron pentacarbonyl is in its ground state or at least with a minor proportion of higher energy conformations.

Recently published theoretical results predict an optimal square pyramid geometry $C_{4v}$ for the $Fe(CO)_5^+$ structure.[30] Vibrational fine structures have long been recognized to give reliable indications of the geometry of ionic states in the case of other carbonyl metal compounds.[31,32] In fact, intermolecular rearrangement from $D_{3h}$ to $C_{4v}$ symmetry is characterized by a transformation of the e′ and e″ levels of the 3d metal orbitals into three different levels $b_2$, e, $a_1$, for which two different energy orderings have been proposed.[22] However, our experimental spectrum does not give such a definite answer. On the other hand, the interpretation of the TPE spectrum allows the unequivocal assignment of the symmetry of the neutral molecule.

Two kinds of ionization processes are usually considered.

**Adiabatic.** This corresponds to a transition from the vibrational level $v = 0$ of the neutral molecule to the $v = 0$ level of the ionic system. The cross section for this process is low when it is associated with a large change in geometry (lowest energy transitions, onset of each PES band).

**Vertical.** In this case the IP is the energy required to remove an electron without any nuclear geometry change (largest Franck−Condon factors, maximum of the PES bands).

The width of a single band is related to the energy difference between points on the potential energy surface of the ion: the equilibrium geometry of the neutral species and that of the ion itself. Due to the fact that the electron removed in the lowest energy ionizations is a nonbonding or weakly bonding electron, the vertical IP is expected to be close to the adiabatic one, leading to relatively narrow bands.

Lloyd et al.[6] have given a qualitative interpretation of the lowest PES bands based on simple calculations of the energy splitting between the e′ and e″ levels (vertical process is considered). They assign the first band (8.60 eV) to the e′ level and the second band (9.86 eV) to the e″ level of the d metal orbitals. Interpretation of the He* Penning ionization electron spectrum (PIES) has been based on the band strength with orbital density on the molecular surface.[13] This interpretation of the metal d bands confirms the preceding one.

An ambiguity remains for the "internal" orbitals. Discrete variational Xα calculations[12,13] and higher level studies by M. Ohno et al.[33] using the Green's function method have been done: the calculated IPs are in good agreement with the experimental ones, but the origin of the bands in term of specific metal or ligand MOs has not been clarified. In the theoretical part of this paper we try to fill this deficiency.

## 4. Theoretical Determination of the Ionization Potentials

The lowest level approximation for the evaluation of the IPs is provided by the well-known Koopmans theorem.[19] This approximation may be rather poor because no relaxation of the MOs is allowed after the ionization process and the difference between the correlation energies of the neutral molecule and the ion is not taken into account. However the two effects tend to cancel each other[34] so that the Koopmans theorem usually gives acceptable results, or at least it is a good starting point for more precise approximations.

The ion repolarization effect can be considered by performing SCF calculations on the ion (ΔSCF method). Unfortunately, except when the hole is in the HOMO of each symmetry, it may be difficult to achieve the convergence of the SCF procedure. In the Xα calculations[12,35] performed on $Fe(CO)_5$, the repolarization effect has been partially taken into account by means of the Slater transition state method[36,37] (STSM). The STSM consists essentially of using an occupation number of one-half for the spin−orbital from which the electron is taken away. The new orbital energy represents a better evaluation of the IP than that obtained from Koopmans' theorem because a fractional occupation number causes the other $n - 1$ electrons to feel an intermediate situation between the neutral molecule and the ion. Some problems of convergence can be found in this case too. A third way to introduce part of the repolarization effect is to perform a CI calculation including all single excitations from occupied to virtual orbitals, with respect to a given $n - 1$ electron Slater determinant describing the ion in the Koopmans approximation[38] (Koopmans−Slater determinant, KSD). This procedure has been already applied for transition metal compounds in the case of inner-shell IPs.[39] Notice that the SCF Slater determinant (SSD) of the ion and the monoexcitations with respect to it do not interact (Brillouin theorem). If we consider a different Slater determinant approximating the SSD, such as the KSD, the contribution to the CI wave function of the monoexcitations may be interpreted as an improvement of the molecular orbitals rather than a description of the electronic correlation.[40−42]

Another problem arises in the frame of Koopmans' theorem calculations on $Fe(CO)_5$. Due to the high symmetry, the canonical MOs are completely delocalized on the molecule, thus

complicating the attribution of the observed photoionization bands. If the nature of the orbital from which the electron has been extracted in the KA is understood, it becames easy to correlate the PES to the electronic structure of the metal center and of the ligands. This facilites the interpretation of PE spectra of analogous compounds with other ligands or metals. Different approaches can be considered in order to obtain localized orbitals from the canonical ones. We have applied a procedure recently proposed by one of us.[43] The doubly occupied canonical SCF molecular orbitals (CMOs) undergo a unitary transformation in order to produce physically meaningful localized quasi-bond orbitals (QBOs), as similar as possible to a set of completely localized nonorthogonal bond orbitals (BOs). BOs are obtained by Del Re's method[44] in its ab initio version.[43] The unitary transformation from CMOs to QBOs is performed so as to maximize the sum of the square overlaps of each QBO with the corresponding BO (for mathematical details of the procedure, see ref 45).

With respect to other localized orbitals, the QBOs have the advantage of describing the molecule in "chemical" terms, such as bonds and lone pairs, but they do not satisfy Koopmans' theorem (only the CMOs do[46]); however, it can be shown[20] that Koopmans' IPs can be obtained from a CI calculation involving all the $(n-1)$-electron KSDs built up on a basis of noncanonical orbitals. When the CI is based on QBOs, the CI coefficients are the elements of the unitary transformation from the CMOs to the QBOs. In a quasi-particle picture, this procedure enables us to express the Koopmans IPs as the energy required to remove an electron from an orbital which is a linear combination of QBOs and therefore to assign the observed photoionization bands.

As a further step, the correlation effect has to be evaluated in a MO−CI scheme. Owing to the number of valence electrons and the dimension of the basis set, a high quality CI treatment for neutral and ionic $Fe(CO)_5$ is computationally very demanding. We have chosen to perform single and double CI calculations (SDCI) using selected excited determinants. We use the canonical SCF MOs of neutral $Fe(CO)_5$ as a one-electron basis set both for $Fe(CO)_5$ and for $Fe(CO)_5^+$. The calculations have been carried out by means of the Pisa modified CIPSI program.[47,48] The determinants used in SDCI have been selected according to the philosophy of the CIPSI algorithm, using the threshold $\eta_S = 0.0025$.

## 5. Computational Details

Ab initio SCF calculations have been performed using the HONDO8 program.[49] For the Fe atom we use the (14s, 9p, 5d) primitive Gaussian set of Wachters[50] reduced to [8s, 4p, 3d] by using his contraction scheme 2. We have added two p functions to describe the 4p orbitals according to Wachters[51] and one diffuse d function as indicated by Hay.[52] The final basis set for Fe is [8s, 6p, 4d]. For C and O atoms the (9s, 5p) primitive Gaussian basis set of van Duijneveldt[53] is reduced to [4s, 3p] using the contraction scheme (5211) for s functions and (311) for p functions.

For the trigonal bipyramid geometry of $Fe(CO)_5$, the bond lengths are those of Barnes,[54] optimized by the modified coupled-pair functional (MCPF) method. For the square pyramid geometry, we have used the bond lengths obtained by Ricca and Bauschlicher[30] for the $Fe(CO)_5^+$ ion. The basis sets (and methods) employed in the two geometry optimizations are different, but we can safely assume that the final interpretation of our results would not be affected by small changes in the bond lengths, preserving the molecular symmetry.

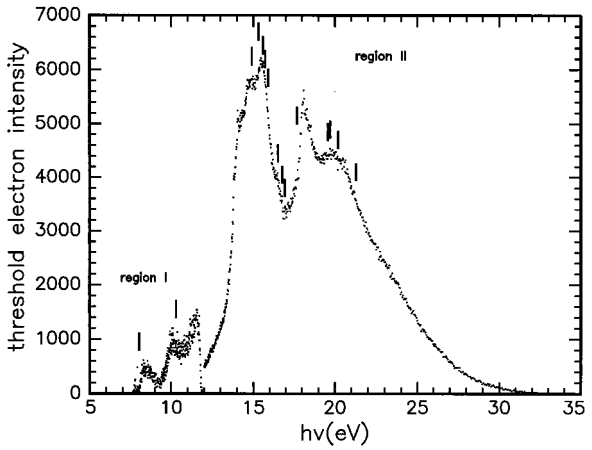


**Figure 1.** TPES of $Fe(CO)_5$ in the photon energy range 5−35 eV. The first region, I, corresponding to the iron orbitals, has been registered with a LiF cutoff window; the second region, II, corresponding to CO molecular orbitals, has been registered without a LiF cutoff window. The TPE spectrum has not been normalized by the light intensity. The plotted marks correspond to the SDCI calculated values reported in Table 2 (see text).

## 6. Threshold Photoelectron Spectrum of $Fe(CO)_5$ and ab Initio Calculations

The TPE spectrum of $Fe(CO)_5$ is shown in Figure 1. This spectrum has been registered in two parts, one with a LiF window cutoff (in the 5−11.8 eV energy range) and the other without cutoff (in the 11.8−35 eV energy range). The HeI PE spectrum of $Fe(CO)_5$ has already been reported,[6,7,12] the only published TPES being registered in the 13−19 eV range.[7] The TPES presents the same structures as the HeI PES,[6,12] particularly in that no Franck−Condon gap is distinguishable, while resonant autoionization processes are observed in the case of the chromium hexacarbonyl,[55] $Cr(CO)_6$. The lack of autoionization structures in the TPES is consistent with the likely rapid dissociation of expected excited $Fe(CO)_5$ and $Fe(CO)_5^+$ in the studied energy region.

The structure of the TPE spectrum is in agreement with the one generally resolved in the HeI PE spectrum. The region of lowest energy below 11.8 eV (LiF cutoff) contains the Fe 3d ionization potentials. The system of overlapping bands in the region 11.8−30 eV likely corresponds to ligand MOs.

Let us consider first the metal 3d IPs. According to the MO theory, in a $D_{3h}$ symmetry, the Fe 3d orbitals are split into one unoccupied $a_1'$ ($3d_{z^2}$) orbital and two filled sets of degenerate orbitals, the e′ ($3d_{x^2-y^2}$, $3d_{xy}$) and e″ ($3d_{xz}$, $3d_{yz}$) levels. A previous theoretical estimate of 1.6 eV for the difference between the e′ and e″ ionization potential[6] is in agreement with the 1.3 eV PE experimentally observed splitting.[6,12]

From the TPE spectrum the vertical IPs for the e′ and e″ levels are 8.3 and 10.1 eV, respectively. The e′ and e″ adiabatic IPs can be evaluated at 8 and 9.4 eV respectively. In Table 1 we report some examples of previously observed values of the first and second IP along with the absolute value of the calculated orbital energies of these occupied metal d levels.

The values of the calculated IPs in the KA are higher than the observed PE ones by 1.3 (e′) and 3.4 (e″) eV. Similar calculations on the square pyramid geometry ($C_{4v}$) give 5.9, 13.7, and 14.1 eV for the iron 3d electrons. This rules out the square pyramid conformation as the starting geometry in the photoionization process.

In Table 2 we report all the Koopmans IPs in the energy interval under study. They are in approximate agreement with those of ref 33.

**TABLE 1: Observed Values of the First and Second Ionization Bands and Calculated IPs for the e′ and e″ Levels for Metal d Orbitals (See Text)**

| method | e′ IP (eV) | e″ IP (eV) |
|---|---|---|
| experimental | | |
| PES[6,12] | 8.6 | 9.9 |
| TPES vertical (this work) | 8.3 | 10.1 |
| TPES adiabatic (this work) | 8.0 | 9.4 |
| theoretical (this work) | | |
| SCF−Koopmans (KA) | 9.6 | 13.5 |
| SCF STSM | 8.7 | |
| ΔSCF | 5.6 | 7.4 |
| single-$CI_{ion}$ on neutral COs | 5.3 | 6.3 |
| ΔSDCI | 8.0 | 10.3 |
| theoretical (previous) | | |
| Xα STSM[35] | 8.2 | 9.6 |
| Xα STSM[12] | 7.7 | 9.0 |
| Xα STSM[12] | 9.0 | 10.2 |
| Xα[63] | 8.87 | 9.83 |
| INDO−Koopmans[64] | 9.01 | 10.33 |
| SCF−Koopmans[54] | 7.75 | |
| Green's function method[33] | 8.6 | 9.9 |

**TABLE 2: Comparison between Experimental IPs and Calculations with Different Methods (See Text)**

| orbital | KA | single-$CI_{ion}$ | ΔSDCI | $IP_{exp}$[a,b] | $IP_{exp}$ − ΔSDCI |
|---|---|---|---|---|---|
| 10e′ | 9.6 | 5.3 | 8.0 | 8.3(m) | 0.3 |
| 3e″ | 13.5 | 6.3 | 10.3 | 10.1(m) | −0.2 |
| $8a_2''$ | 16.6 | 16.3 | 14.9 | 14.0(s) | −0.9 |
| $13a_2''$ | 16.8 | 15.0 | 14.9 | 14.9(s) | 0.0 |
| 2e″ | 17.2 | 15.8 | 15.7 | | |
| 9e′ | 17.2 | 16.0 | 15.3 | 15.5(m) | 0.2 |
| $1a_2'$ | 17.4 | 16.1 | 15.6 | 15.6(s) | 0.0 |
| 8e′ | 17.7 | 16.3 | 15.9 | | |
| 7e′ | 18.4 | 17.4 | 16.8 | | |
| $7a_2''$ | 18.5 | 17.5 | 16.5 | 16.5(s) | 0.0 |
| 1e″ | 18.5 | 17.4 | 16.9 | | |
| $12a_1'$ | 19.8 | 19.1 | 17.7 | 18.1(m) | 0.4 |
| 6e′ | 22.0 | 20.2 | 19.6 | | |
| $11a_1'$ | 22.1 | 21.4 | 19.7 | 19.8(m) | 0.1 |
| $6a_2''$ | 22.7 | 21.1 | 20.2 | 20.5(s) | 0.3 |
| $10a_1'$ | 23.7 | 22.9 | 21.3 | 21.2(s) | −0.1 |

[a] (m): maximum, (s): shoulder. [b] Each experimental IP has been arbitrarily assigned to the orbital closest in energy in the SDCI scheme. This assignment is of course not the only possible one.

For the peaks unequivocally identified in the experimental spectrum (Figure 1), KA overestimate the IPs by 1.9−2.5 eV. The weakness of the KA indicates that relaxation is important for this system and that electron correlation does not completelly compensate for it. According to Ohno et al.[33] charge transfer is of great importance in this system, leading to a breakdown of the quasi-particle picture.

Before introducing more refined approximations, we present a decomposition of the CMOs in term of QBOs. Clearly this analysis, being based on the KA, can only be a qualitative help for the attribution of the bands. Moreover, it gives a picture of the electronic distribution in the neutral molecule at the SCF level.

We have performed a localization of the CMOs as indicated in section 4. The BOs are simply the orbitals of the fragments (Fe and CO). An SCF calculation on the isolated iron atom gives the reference metal orbitals (the occupation numbers are 1.4 for the 3d orbitals and 1.0 for the 4s orbital, halfway between those appropriate for the $4s^23d^6$ atomic ground state and for the $3d^8$ configuration found in the molecular surrounding[23,56]). We include in the reference BO space the $3d_{x^2-y^2}$, $3d_{xy}$, $3d_{xz}$, and $3d_{yz}$ orbitals. The BOs describing the ligands are obtained by Del Re's method,[43] as indicated in section 4.

The localization is well achieved: in Table 3 we report the values of the least and mean square overlaps between the QBOs

**TABLE 3: Overlaps between the (Quasi-Localized) Quasi-Bond Orbitals and the Reference (Fully Localized) Bond Orbitals (See Text)**

| type of orbital | least overlap | mean square overlap |
|---|---|---|
| $d_{xy}$, $d_{x^2-y^2}$, Fe (e′) | 0.9031 | 0.8156 |
| $d_{xz}$, $d_{yz}$ Fe (e″) | 0.9804 | 0.9610 |
| π CO | 0.9908 | 0.9822 |
| lp C | 0.9384 | 0.8850 |
| lp O | 0.9871 | 0.9744 |
| σ CO | 0.9707 | 0.9425 |
| 1s, 2s, 2p, 3s, 3p Fe | | |
| 1s O, 1s C | 0.9998 | 1.000 |

(obtained by unitary transformation of the CMOs[43]) and the totally localized BOs. The e′ orbitals are not perfectly spanned by the reference BO basis. We note that weak overlaps arise because of two different effects: the first is the distortion of the metal and ligand orbitals in the molecular environment, and the second is the formation of dative bonds (ligand−metal donation an back-donation). The orbital distortion does not affect the attribution of the QBOs to the various fragments.

As said before, the reference e′ orbitals simply are the $d_{xy}$, $d_{x^2-y^2}$ orbitals of the isolated Fe atom because no hybridization is supposed to be relevant for these orbitals. In the molecular surroundings they are distorted by the presence of the three equatorial CO ligands, because of the interaction with the carbonyl lone pairs and because of the metal-d to CO-$\pi^*$ donation. The better overlap of the $d_{xz}$ and $d_{yz}$ orbitals with the reference atomic orbitals indicates that they are less modified by the presence of the carbonyls and less involved in the d → $\pi^*$ back-donation to CO, in agreement with Hoffmann's results.[23] The lone pairs of CO are also not completely well spanned. We note that the e′ orbitals and CO lone pairs, although being modified because of the perturbation in the molecular surroundings, remain localized on the fragments. Indeed, the distortion mainly involves the virtual orbitals of the same fragment and only to a little extent is due to a mixing with orbitals of the other fragments.

It is also important to note that the $3d_{z^2}$, 4s, and 4p orbitals are not included in the BO reference space of the metal. This means that no ligand to metal σ donation is described by the reference BOs. The quite large overlap between the carbon lone pair QBOs and the corresponding BOs shows that σ donation, although appreciable, is not really large (for the relative importance of ligand to metal σ donation and ligand to metal π donation to bond energies, see ref 56). The other orbitals give overlaps close to one; that is they are practically unperturbed by the other fragments.

In Table 4 we present the composition of the CMOs in term of QBOs. We use the notation $\pi^{\parallel}$ and $\pi^{\perp}$ to indicate the equatorial CO π ligand orbitals with nodal planes respectively orthogonal and parallel to the molecular equatorial plane. Only a few CMOs are well described by one specific type of fragment orbital; however there is a clear distinction between metal and ligand orbitals. As expected, the 10e′ and 3e″ orbitals have essentially metal 3d character with minor components on the equatorial lone pairs (10e′) and on the equatorial $\pi^{\perp}$ and axial π (3e″) ligand orbitals. In some cases it is possible to assign the orbitals to local σ ($13a'$, $12a_1'$,$1e''$,$11a_1'$,$6a_2''$, $10a_1'$) or π ($2e''$,$1a_2'$) symmetry of the CO fragments. In the other cases the orbitals are mixtures of different local symmetry CO orbitals. Moreover the bonding σ CO orbitals are not much involved in the IPs under consideration. We note that our decomposition overcomes the artifacts of Mulliken's population analysis (MPA), which arise when diffuse basis functions are used. In the present system diffuse functions needed to describe 4s and 4p orbitals make the MPA quite unreliable, as pointed out by

**TABLE 4: Percent Composition of the Canonical Orbitals in Terms of Quasi-Bond Orbitals (See Text)**

| canonical orbital | iron | | equatorial CO | | | | | axial CO | | | |
|---|---|---|---|---|---|---|---|---|---|---|---|
| | 3d e′ | 3d e″ | $\pi^{\parallel}$ | $\pi_{\perp}$ | lp C | lp O | $\sigma$ CO | $\pi$ | lp C | lp O | $\sigma$ CO |
| 10e′ | 81.9 | | 2.1 | | 15.1 | 0.5 | 0.3 | 0.2 | | | |
| 3e″ | | 90.3 | | 5.6 | | | | 4.1 | | | |
| $8a_2''$ | | | | 66.0 | | | | | 28.7 | 3.5 | 1.6 |
| $13a_1'$ | | | | | 45.0 | 8.2 | 4.1 | | 36.3 | 4.5 | 2.0 |
| 2e″ | | 1.8 | | 79.7 | | | | 15.5 | | | |
| 9e′ | 7.2 | | 15.2 | | 39.8 | 10.5 | 5.1 | 22.3 | | | |
| $1a_2'$ | | | 100.0 | | | | | | | | |
| 8e′ | 7.6 | | 81.7 | | 6.3 | 2.3 | 1.0 | 1.0 | | | |
| 7e′ | 1.5 | | 1.0 | | 11.3 | 7.4 | 3.1 | 75.8 | | | |
| $7a_2''$ | | | | 33.0 | | | | | 44.8 | 15.1 | 7.1 |
| 1e″ | | 8.0 | | 14.6 | 77.4 | | | | | | |
| $12a_1'$ | | | | | 8.8 | 30.5 | 9.9 | | 22.5 | 20.7 | 7.7 |
| 6e′ | 1.8 | | | | 26.0 | 64.6 | 6.9 | 0.8 | | | |
| $11a_1'$ | | | | | 17.3 | 35.8 | 3.6 | | 2.2 | 35.3 | 5.8 |
| $6a_2''$ | | | | 0.9 | | | | | 24.8 | 67.3 | 7.0 |
| $10a_1'$ | | | | | 26.3 | 10.7 | | | 36.9 | 25.3 | 0.8 |

Bauschlicher.[56] Notice that Tables 3 and 4 supply complementary information: the former concerns the actual localization of the QBOs, while the latter contains the composition of the CMOs in terms of the (quasi-localized) QBOs.

The relaxation effect has been considered by the STSM and the ΔSCF methods (Table 1). In both cases the convergence has been reached only for ionization from the highest orbitals. The STSM 10e′ IP is in good agreement with the experimental one and with the best Xα STSM values. The ΔSCF 10e′ and 3e″ IPs are surprisingly low, which indicates a large relaxation effect of the ion, which should be compensated for the most part by the electron correlation.

It is clear that the double degeneracy of the 10e′ (or 3e″) orbitals is not preserved in the ion when the orbitals have different occupation numbers. In this case the trigonal bipyramid is not the stable geometry for the ion, because of a Jahn−Teller effect, leading to a square pyramid geometry for the $Fe(CO)_5^+$ ground state.[30]

Monoexcitation CI on KSDs is another way to evaluate the relaxation effect. This useful, albeit approximate, approach enables one to estimate the relaxation effect even for inner holes. We present in Tables 1 and 2 the obtained IPs (single $CI_{ion}$). The comparison with the available ΔSCF 10e′ and 3e″ values shows that this approach gives the correct order of magnitude of the relaxation effect, although slightly overestimated. The agreement with experiment is improved with respect to KA; only the $11a_1'$ and $10a_1'$ have an error greater than 1.5 eV.

A further improvement can be obtained by including the correlation effect. The values of Table 2, computed from a truncated SDCI scheme, are relatively close to those reported using Green's function method.[33]

As appears from the experimental TPES shown in Figure 1, only 11 of the 16 expected IPs are detected as maxima or shoulders in the spectrum. Each of these experimentally detectable maxima can be assigned to one of the (ΔSDCI) values within 0.9 eV or less, except those at 14−15 eV. Therefore, the various refinements of Koopmans' approximation lead to a very satisfying agreement between theoretical IPs and available experimental data. An interesting consideration can be made at this point. As said in section 4, the usual explanation of the relatively good quality of the KA is that relaxation and correlation effects are often of the same magnitude and with different sign. It is clear that relaxation always decreases Koopmans' IPs. On the other hand the correlation energy is usually greater for the neutral systems than for the ionic ones, owing to the larger number of electrons. Our separate estimate of the two effects shows that these considerations are valid for metal 3d IPs (although the first is larger in magnitude), while for ligand orbitals both effects decrease the IP values with respect to Koopmans' approximation.

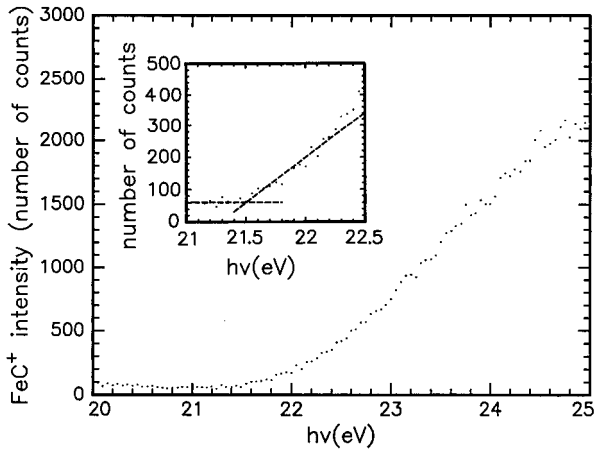


**Figure 2.** $FeC^+$ appearance threshold spectrum registered in the 20−25 photon energy range. In the inset: detail of the 21−22.5 eV region, showing an approximate determination of the apparent threshold using a linear fit of the curve between 21.5 and 22.5 eV (see text).

### 7. $FeC^+$ Appearance Threshold

The ionization efficiency for the $FeC^+$ production is plotted in Figure 2 for photon energies between 20 and 25 eV. In the inset of Figure 2, one can see that the apparent threshold for the $FeC^+$ formation is close to 21.5 eV. This energy range is in agreement with the value of 23.6 eV measured by electron impact a few years ago.[10] The threshold for formation of $CrC^+$ from chromium hexacarbonyl is also reported to be larger than 20 eV.[55]

The temperature of the neutral precursor, $Fe(CO)_5$, in this photoionization experiment is about 300 K. Since it has been shown[57,58] that for most molecules a large fraction of the mean thermal energy $\langle E_{Th} \rangle$, stored in the neutral molecule at a temperature $T$, is effective in the dissociation process, one has to take it into account in order to extract the 0 K dissociation threshold. We assume a linear shape for the 0 K ionization efficiency curve, $A(E_{h\nu} - E_s)$, where $A$ is a constant, $E_{h\nu}$ the photon energy, and $E_s$ the 0 K threshold (which seems not unreasonable in the present case), and then we easily evaluate the ionization efficiency curve at a temperature $T$ by convoluting the 0 K shape with the Boltzmann internal energy distribution: $P(E_i) = CN(E_i) \exp(-E_i/kT)$, where $C$ is the normalization constant, $N(E_i)$ the density of rovibrational states in the molecule, and $k$ the Boltzmann constant.[57,58] We use here the Stein−

Rabinovitch algorithm[59] together with experimental vibrational constants[60] to calculate the density of states $N(E_i)$. One can deduce a value of about 0.28 eV for the average thermal energy $\langle E_{Th} \rangle$ of $Fe(CO)_5$ at a temperature of 300 K. For a photon energies above the 0 K threshold ($E_{h\nu} > E_s$) the convoluted curve is a nearly straight line that intercepts the $x$ axis at $E_{h\nu} = E_s - \langle E_{Th} \rangle$. At photon energies below $E_s$, the convoluted curve deviates from linearity and tails off to zero.

An easy way to evaluate the 0 K threshold, $E_s$, is to extrapolate the linear part of the curve to zero[57,58] to get $E_s - \langle E_{Th} \rangle$. We did the extrapolation using lower and upper bounds of the photon energy for the fit between 21.5 and 22.5 eV. We obtained an intercept of the $x$ axis for photon energies that ranges between 21.5 and 21.7 eV, due to the scatter of data and to the difficulty of choosing the lower bound (one has to estimate at what energy the curve starts deviating from linearity). Adding $\langle E_{Th} \rangle = 0.28$ eV, one gets a mean 0 K dissociation threshold close to 21.9 eV.

Another way to derive $E_s$ is to fit the entire experimental curve, i.e., for photon energies both above and below $E_s$, by the calculated convolution of $A(E_{h\nu} - E_s)$ and $P(E_i)$. The two unknowns, $A$ and $E_s$, are directly extracted from the fit. This method has the advantage that the lower bound is no more the point from which the curve deviates from linearity and can be safely chosen below the apparent threshold. However, we still have to choose the upper bound of the fit that we have limited to 22.5 eV. One derives by this method a final value for $E_s$ of $21.84 \pm 0.1$ eV. This corresponds to the appearance photon energy at 0 K of $FeC^+ + O + 4CO + e^-$ from $Fe(CO)_5$.

Assuming that there is no energetic barrier to $FeC^+$ formation from $Fe(CO)_5^+$, this result allows one to derive the 0 K bond dissociation energy of $FeC^+$, $D_0(Fe^+-C)$. Using the appearance energy of $Fe^+$ from $Fe(CO)_5$ ($14.383 \pm 0.067$ eV,[7] reported with a lower uncertainty than in ref 8) and the bond dissociation energy of CO ($256.16 \pm 0.2$ kcal/mol) obtained from the 0 K heats of formation of C, O, and CO,[61] one obtains $D_0(Fe^+-C) = 84.2 \pm 4.1$ kcal/mol. This value leads to the corresponding 0 K heat of formation of $FeC^+$, $\Delta H_f(FeC^+) = 366.0 \pm 6.0$ kcal/mol, using the reported 0 K heats of formation of gaseous $Fe^+$ and C.[61]

A previous determination[4] of $D_0(Fe^+-C)$, along with $D_0(Fe^+-CH_2)$, was performed using photodissociation of $FeCH_2^+$ and yielded $D_0(Fe^+-C) = 94 \pm 7$ kcal/mol. The value determined in this work is slightly lower, but the two results, although obtained by very different ways, are consistent.

## 8. Conclusions

For the first time the TPES of $Fe(CO)_5$ has been measured over a wide range of energies (5−35 eV): its main features are similar to those of the PES. By means of quantum-mechanical calculations it has been possible to assign most of the observed transition bands in the $Fe(CO)_5$ photoionization spectrum. Although more accurate calculations might yield a better agreement, our purpose was to give a clear interpretation of the observed TPES bands. Further improvement of the calculated IPs with this atomic basis set needs the inclusion of a large number of determinants in the CI calculation, thus increasing the computational effort without making the interpretation easier.

Our approach, perhaps less accurate than that of ref 33, is attractive because good values are obtained as successive improvements over Koopmans' IPs, from which an interpretation of the origin of the bands is clear. Our results are also relevant to the discussion on the validity of Koopmans' theorem and on the way to improve it.

The 0 K appearance threshold for formation of $FeC^+$ from $Fe(CO)_5$ has been accurately determined by fitting the $FeC^+$ intensity curve. The corresponding 0 K BDE value, $D_0(Fe^+-C) = 84.2 \pm 4.1$ kcal/mol at 0 K, confirms the high strength of the corresponding bond.

**Acknowledgment.** The authors wish to thank M. Persico (University of Pisa) for invaluable commentaries and suggestions and H. Mestdagh (Ecole Normale Supérieure, Paris) for a critical examination of this work. We are grateful to the LURE staff for operating the ACO storage ring and the general facilities.

## References and Notes

(1) Weishaar, J. C. *Adv. Chem. Phys.* **1992**, *82*, 213.
(2) Armentrout, P. B. *Annu. Rev. Phys. Chem.* **1990**, *41*, 313.
(3) Eller, K.; Schwarz, H. *Chem. Rev.* **1991**, *91*, 1121.
(4) Hettich, R. L.; Freiser, B. S. *J. Am. Chem. Soc.* **1986**, *108*, 2537.
(5) Distefano, G. *J. Res. Natl. Bur. Stand. Sect. A* **1970**, *74*, 233.
(6) Lloyd, D. R.; Schlag, E. W. *Inorg. Chem.* **1969**, *8*, 2544.
(7) Norwood, K.; Ali, A.; Flesh, G. D.; Ng, C. Y. *J. Am. Chem. Soc.* **1990**, *112*, 7502.
(8) Fieber-Erdmann, M.; Holub-Krappe, E.; Bröker, G.; Dujardin, G.; Ding, A. *Int. J. Mass Spectrom. Ion Processes* **1995**, *149/150*, 513.
(9) Winters, R. E.; Kiser, R. W. *Inorg. Chem.* **1964**, *3*, 699.
(10) Bidinosti, D. R.; McIntyre, N. S. *Can. J. Chem.* **1967**, *45*, 641.
(11) Schultz, R. H.; Crelin, K. C.; Armentrout, P. B. *J. Am. Chem. Soc.* **1991**, *113*, 8590.
(12) Baerends, E. J.; Oudshoorn, Ch.; Oskam, A. *J. Electron Spectrosc. Relat. Phenom.* **1975**, *6*, 259.
(13) Harada, Y.; Ohno, K.; Mutoh, H. *J. Chem. Phys.* **1983**, *79*, 3251.
(14) Niles, S.; Prinslow, D. A.; Wight, C. A.; Armentrout, P. B. *J. Chem. Phys.* **1990**, *93*, 6186.
(15) Barnes, L. A.; Rosi, M.; Bauschlicher, C. W. *J. Chem. Phys.* **1990**, *93*, 609.
(16) Berthier, G.; Cimiraglia, R.; Daudi, A.; Mestdagh, H.; Rolando, C.; Suard, M. *J. Mol. Struct. (THEOCHEM)* **1992**, *254*, 43.
(17) Castro, M.; Salahub, D. R.; Fournier, R. *J. Chem. Phys.* **1994**, *100*, 8233.
(18) Kasai, Y.; Obi, K.; Ohshima, Y.; Endo, Y.; Kawaguchi, K. *J. Chem. Phys.* **1995**, *103*, 90.
(19) Koopmans, T. *Physica* **1933**, *1*, 104.
(20) Newton, M. D. *J. Chem. Phys.* **1968**, *48*, 2825.
(21) Dutuit, O.; Alcaraz, C.; Gerlich, D.; Guyon, P. M.; Hepburn, J.; Métayer-Zeitoun, C.; Ozenne, J. B.; Schweizer, M.; Weng, T. *Chem. Phys.* **1996**, *209*, 177.
(22) Demuynck, J.; Strich, A.; Veillard, A. *Nouv. J. Chim.* **1977**, *1*, 217.
(23) Rossi, A.; Hoffmann, R. *Inorg. Chem.* **1975**, *14*, 365.
(24) Dartiguenave, M.; Dartiguenave, Y.; Gray, H. B. *Bull. Soc. Chim. Fr.* **1969**, *12*, 4223.
(25) Elian, M.; Hoffmann, R. *Inorg. Chem.* **1975**, *14*, 1058.
(26) Almenningen, A.; Haaland, A.; Wahl, K. *Acta Chem. Scand.* **1969**, *23*, 2245.
(27) Davis, M. I.; Hanson, H. P. *J. Chem. Phys.* **1965**, *69*, 3405.
(28) Spiess, H. W.; Grosescu, R.; Haeberlen, U. *Chem. Phys.* **1974**, *6*, 226.
(29) Berry, R. S. *J. Chem. Phys.* **1960**, *32*, 933.
(30) Ricca, A.; Bauschlicher, C. W. *J. Phys. Chem.* **1994**, *98*, 12899.
(31) Hubbard, J. L.; Lichtenberger, D. L. *J. Am. Chem. Soc.* **1982**, *104*, 2132.
(32) Reutt, J. E.; Wang, L. S.; Lee, Y. T.; Shirley, D. A. *Chem. Phys. Lett.* **1986**, *126*, 399.
(33) Ohno, M.; von Niessen, W. *J. Chem. Phys.* **1991**, *95*, 373.
(34) Mulliken, R. S. *J. Chim. Phys.* **1949**, *48*, 497.
(35) Guerra, M.; Jones, D.; Distefano, G.; Foffani, A.; Modelli, M. *J. Am. Chem. Soc.* **1988**, *110*, 375.
(36) Slater, J. C. *Adv. Quantum Chem.* **1972**, *6*, 1.
(37) Beebe, N. H. F. *Chem. Phys. Lett.* **1973**, *19*, 290.
(38) Pauzat, F.; Ridard, J.; Millié, Ph. *Mol. Phys.* **1972**, *24*, 1039.
(39) Decleva, P.; Fronzini, G.; Lisini, A.; Stener, M. *Chem. Phys.* **1994**, *186*, 1.
(40) Lefebvre, R.; Moser, C. M. *J. Chim. Phys.* **1956**, *53*, 393.
(41) Lefebvre, R. *J. Chim. Phys.* **1957**, *54*, 168.
(42) Lefebvre, R. *Cah. Phys.* **1959**, *13*, 369.
(43) Angeli, C.; Del Re, G.; Persico, M. *Chem. Phys. Lett.* **1995**, *233*, 102.
(44) Del Re, G. *Theor. Chim. Acta (Berlin)* **1963**, *1*, 188.
(45) Persico, M. *Spectral Line Shapes*; Rostas, F., Ed.; De Gruyter: Berlin, 1985; Vol. 3, pp 587−613.
(46) Angeli, C. *J. Chem. Ed.*, submitted

(47) Huron, B.; Malrieu, J. P.; Rancurel, P. *J. Chem. Phys.* **1973**, *58*, 5745.
(48) Cimiraglia, R.; Persico, M. *J. Comput. Chem.* **1987**, *8*, 39.
(49) Dupuis, M.; Farazdel, A.; Karna, S. P.; Maluendes, S. A. *MOTECC 1990*; Clementi, E., Ed.; ESCOM: Leiden, 1990; pp 277−342.
(50) Wachters, A. J. H. IBM Technical Report, RJ 584, San Jose, CA, 1969.
(51) Wachters, A. J. H. *J. Chem. Phys.* **1970**, *52*, 1033.
(52) Hay, P. J. *J. Chem. Phys.* **1977**, *66*, 4377.
(53) van Duijneveldt, F. B. IBM Research Report, RJ 945 San Jose, CA, 1971.
(54) Barnes, L. A.; Rosi, M.; Bauschlicher, C. W. *J. Chem. Phys.* **1991**, *94*, 2031.
(55) Das, P. R.; Nishimura, T.; Meisels, G. G. *J. Phys. Chem.* **1985**, *89*, 2808.
(56) Bauschlicher, C. W. *J. Chem. Phys.* **1984**, *81*, 5889.
(57) Guyon, P.-M.; Berkowitz, J. *J. Chem. Phys.* **1971**, *54*, 1814.
(58) Chupka, W. A. *J. Chem. Phys.* **1971**, *54*, 1936.
(59) Stein, S. E.; Rabinovitch, B. S. *J. Chem. Phys.* **1973**, *58*, 2438.
(60) Jones, L. H.; McDowell, R. S.; Goldblatt, M.; Swanson, B. I. *J. Chem. Phys.* **1972**, *57*, 2050.
(61) Chase, M. W., Jr.; Davies, C. A.; Downey, J. R., Jr.; Frurip, D. J.; McDonald, R. A.; Syverud, A. N. *J. Phys. Chem. Ref. Data* **1985,** *14* Suppl. 1.
(62) Baerends, E. J.; Ros, P. *Mol. Phys.* **1975**, *30*, 1735.
(63) Guenzburger, D.; Saitovich, E. M. B. *J. Chem. Phys.* **1984**, *80*, 735.
(64) Kotzian, M.; Rösch, N.; Schröder, H.; Zerner, M. C. *J. Am. Chem. Soc.* **1989**, *111*, 7687.